

# FEEP micro-thrust balance characterization and testing

S Rocca<sup>1</sup>, C Menon<sup>2</sup> and D Nicolini<sup>3</sup>

<sup>1</sup> Department of Mechanical Engineering, University of Padova, via Venezia 1, 35131 Padova, Italy

<sup>2</sup> Advanced Concepts Team, European Space Agency, ESTEC, Keplerlaan 1, 2201 AZ Noordwijk, The Netherlands

<sup>3</sup> European Space Agency, ESTEC, Keplerlaan 1, 2201 AZ Noordwijk, The Netherlands

E-mail: [simone.rocca@unipd.it](mailto:simone.rocca@unipd.it)

Received 9 September 2005, in final form 9 January 2006

Published 10 February 2006

Online at [stacks.iop.org/MST/17/711](http://stacks.iop.org/MST/17/711)

## Abstract

A micro-thrust stand developed by the National Physical Laboratory under ESA funding was calibrated and characterized. The balance is based on the nulled-pendulum principle. The thruster is positioned in a constrained pendulum that is free to move only along the line of thrust. A capacitive displacement sensor measures the movement of the pendulum and is connected via a servo closed loop to a force actuator that preserves the nulled position of the pendulum. The force exerted by the actuator is the measurement of the thrust generated by the field effect electric propulsion thruster. Part of the environmental vibration noise is cancelled by subtracting the signal produced by a dummy pendulum (not subjected to thrust) from the signal produced by the principal pendulum. The interface between the thruster and balance was designed with the aim of minimizing the interference of the electrical wires. This paper presents the results of the measurements that fully characterize the balance in terms of accuracy, resolution and thrust range. Improvements to the balance are suggested in order to increase its metrological performance.

**Keywords:** micro-thrust, direct thrust measurement, thrust balance, space propulsion

(Some figures in this article are in colour only in the electronic version)

## 1. Introduction

Several forthcoming space missions, such as MICROSCOPE (MICROSatellite with drag Control for the Observation of the Equivalence Principle) [1], LISA (Laser Interferometer Space Antenna) [2], LISA Pathfinder (a mission intended to demonstrate the key technologies for LISA) [3] and Darwin (an infrared space interferometry mission) [4], require very accurate satellite position and attitude control. In particular, the mission LISA aims to detect gravitational waves in the frequency range  $10^{-4}$ –2 Hz. In this mission, three identical spacecraft form an equilateral triangle. Each side is 5 million kilometres long and acts as the arm of an interferometer used to detect any relative displacement of test masses free-falling inside the spacecraft. The noise in the micro-thrusters couples

to the gravitational wave signal through the ‘elastic’ coupling of the noisy spacecraft motion to that of the test masses. For this reason, thruster specifications were defined to be: thrust range of 0–100  $\mu\text{N}$ , resolution of 0.1  $\mu\text{N}$  and a noise figure lower than 0.1  $\mu\text{N Hz}^{-0.5}$  in the frequency range  $10^{-4}$ –2 Hz.

The types of thruster deemed to satisfy these requirements are field effect electric propulsion (FEEP) thrusters [5] and colloid thrusters [6]. Both technologies are still under development, and one of the aspects that requires verification is their thrust performance. Therefore, the direct measurement of the thrust generated by these thrusters is a fundamental step in the validation of these technologies and for the successful realization of space missions.

Although direct thrust measurements at micro-Newton levels could not be achieved until a few years ago, several

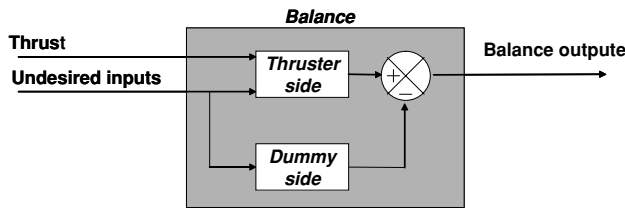


**Figure 1.** Block diagram of the noise cancellation realized with the dummy pendulum.

micro-Newton thrust stands have recently been developed at research centres such as JPL [7], NASA Goddard Space Flight Center [8], ONERA [9], Alenia Spazio-Istituto Colonnetti [10] and Busek [11]. They are either torsional balances or pendulum-based balances.

This paper presents the characterization phase of the FEFP micro-thrust balance that was designed and manufactured by the National Physical Laboratory under an ESA Propulsion Laboratory commission [12]. In order to characterize the balance for space applications, the tests were performed in vacuum ( $10^{-6}$  mbar), and a controlled temperature of 40 °C was maintained (FEFP working temperature).

## 2. Balance description

### 2.1. Principle of operation

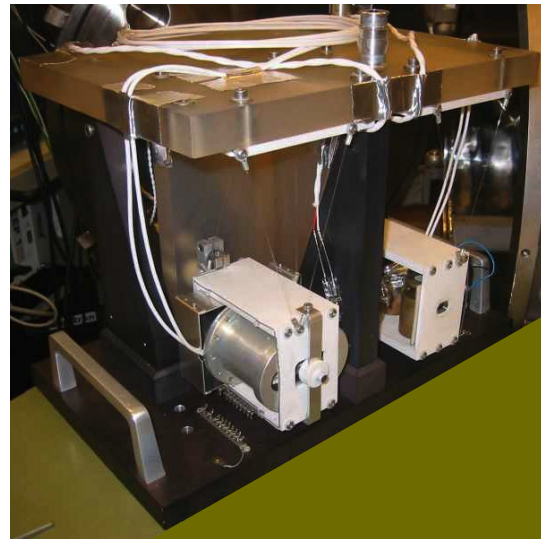
The balance is based on a simple nulled-pendulum principle. The thruster is positioned in a box suspended by wires. The box is free to swing along the direction of thrust only (constrained pendulum). A capacitive displacement sensor (MTI Accumeasure 5000) detects the movement of the pendulum with a resolution of 1 nm and a noise level lower than  $0.1 \text{ nm Hz}^{-0.5}$ . A force feedback control system commanded by the displacement signal exerts the force necessary to counteract the thrust and thus to restore the initial position of equilibrium. The output of the balance corresponds to the force necessary to restore the nulled position.

A dummy pendulum, nominally identical to the first one, is added to the balance as the measurement is very sensitive to tilt and environmental vibrations. A mass equivalent to that of the thruster is positioned on it. The dummy is subjected only to disturbances (thrust acts only on the thruster side). Therefore, subtracting its signal from the thruster pendulum signal compensates and thus reduces the effects of undesired inputs that act on both sides (figure 1). Nevertheless, any difference between the two channels, and any rotational vibrations (which act in an opposite way on the two pendula), still contribute to noise in the measurement.

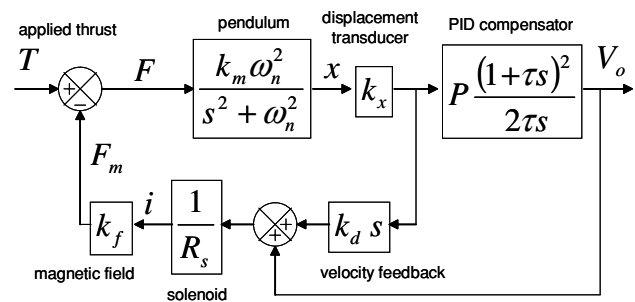
### 2.2. Physical description

Figure 2 shows the balance set-up. Each pendulum consists of a Macor box suspended by five silica fibres. They are connected in such a way that only movement along the direction of thrust is allowed. The fibres are attached to a Zerodur plate. This material was chosen for its very low coefficient of thermal expansion. An aluminium structure supports the Zerodur framework.

One part of the displacement sensor is mounted on the ceramic box, while the other is attached to the Zerodur



**Figure 2.** FEFP micro-thrust balance integrated with a FEFP thruster on the left-hand side. The high-voltage power feeding cables are visible (two on each side). They connect the thruster on the pendulum with the fixed top plate.



**Figure 3.** Block diagram of the balance.  $T$ : applied thrust (N);  $F$ : resultant force on balance (N);  $k_m$ :  $L/(mg)$ ;  $\omega_n$ :  $(g/L)^{0.5}$ ;  $x$ : displacement of the balance (m);  $k_x$ : sensitivity of the displacement transducer ( $\text{V m}^{-1}$ );  $P$ : proportional gain;  $\tau$ : PID time constant (s);  $V_o$ : output signal (V);  $k_d$ : velocity feedback constant;  $R_s$ : constant of proportionality for voltage to current converter ( $\Omega$ );  $i$ : solenoid current (A);  $k_f$ : relates the magnetic force produced by the solenoids to the current ( $\text{N A}^{-1}$ );  $F_m$ : force produced by the solenoids (N);  $m$ : mass of the pendulum including the thruster (kg);  $L$ : effective length of balance suspension (m);  $g$ : acceleration due to gravity ( $\text{m s}^{-2}$ ).

framework. The solenoid/magnet force actuator that realizes the force feedback is mounted in a similar way: the magnet on the box and the solenoid on the Zerodur framework.

FEFP thrusters require high-voltage power supply. For this reason, two high-voltage cables (Reynolds high-voltage coaxial-shielded cables AWG 26) connect the thruster on the pendulum to the fixed part of the balance. The same connection is made on the dummy side in order to recreate the same mechanical interference that the stiffness of the cables exerts on the pendulum.

### 2.3. Servo-control description

Figure 3 shows the block diagram of the balance in which the interfering inputs are neglected as the noise is supposed to be perfectly compensated. It corresponds to the block diagram of one single channel that has thrust as input and  $V_o$  as output.

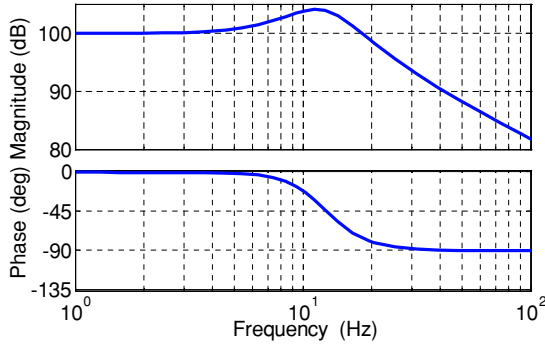


**Figure 4.** Bode plot of the transfer function describing the dynamics of the system.

When an external force  $T$  is applied to the pendulum, a displacement  $x$  is generated. This is converted to a voltage  $V_x$  by the displacement transducer. This voltage is then differentiated and amplified by the velocity feedback unit and passed to the solenoid. In this way, a restoring force proportional to velocity is generated. The constants of the velocity feedback are chosen in such a way as to realize a critical damping. In order to eliminate the steady-state error inherent in a second-order system like the one represented by the pendulum and to realize a true force-nulling system, it is necessary to introduce a pure integration term into the open-loop transfer function. This can be achieved by using a PID compensator. The parameters  $P$  and  $\tau$  are chosen in order to have a dynamical response which is a trade-off between stability and speed of response. From figure 3, it is possible to write the closed-loop transfer function between the output, which is the voltage read, and the input that is the thrust (1):

$$\begin{aligned} \frac{V_0}{T}(s) = & G\{Lk_x P \tau^2 R_s s^2 + 2Lk_x P R_s \tau s + Lk_x P R_s\} \\ & \times \{2m\tau R_s L s^3 + (Lk_x k_f P \tau^2 + 2Lk_x k_f k_d \tau) s^2 \\ & + (2m\tau R_s g + 2Lk_x k_f P \tau) s + Lk_x k_f P\}^{-1}. \end{aligned} \quad (1)$$

In the steady state, the transfer function reduces to

$$\lim_{s \rightarrow 0} \frac{V_0}{T}(s) = G \frac{R_s}{k_f} = 0.1 \text{ V } \mu\text{N}^{-1}. \quad (2)$$

Equation (2) shows that the output signal is proportional to the applied thrust in static conditions. Substituting the numerical values, we obtain the theoretical sensitivity of the balance, which is  $0.1 \text{ V } \mu\text{N}^{-1}$ .

Figure 4 shows the Bode plot of the transfer function describing the dynamics of the system. The plot shows that the instrument can be considered a zero-order system (constant gain and zero phase) in the frequency range 0–3 Hz.

### 3. Experimental results

The experimental set-up as seen in figure 2 was tested in vacuum. A vacuum chamber was prepared for hosting the balance. The vacuum chamber was equipped with two pumps: a turbo-molecular pump for low-vacuum pumping and an ion pump for high-vacuum pumping down to  $7 \times 10^{-7}$  mbar. Only the ion pump was used during the tests, as it does not have mechanical moving parts that could disturb the measurements. The balance was tested at different temperatures in order to

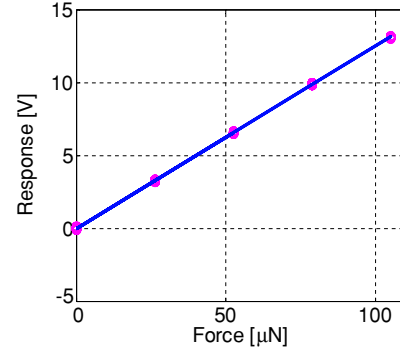


**Figure 5.** Calibration curve (line) and experimental data (circles). The input force is plotted against the corresponding balance output. The balance shows a static sensitivity of  $0.123 \text{ V } \mu\text{N}^{-1}$  and a high linearity (standard uncertainty of  $0.03 \mu\text{N}$ ).

characterize its sensitivity to temperature variations. The temperature in different locations of the balance was controlled by means of four halogen lamps and four temperature sensors (integrated circuits AD590). The thruster and the dummy had a mass of 450 g each.

The balance electronics provides outputs filtered at two frequencies: 1 and 10 Hz. In both cases, an analogue filter is used in order to avoid aliasing phenomena. Measurements were then digitally sampled at 50 Hz. This sampling frequency guarantees to reproduce the frequency content of the filtered signal.

#### 3.1. Static calibration

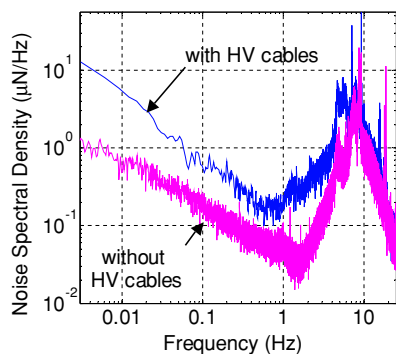
The instrument was calibrated by exerting a known force history with steps ranging from 0 to  $100 \mu\text{N}$  and recording the corresponding output. In this way, the relation between the input (force) and output (voltage) could be determined. The force was exerted by a solenoid/magnet force actuator, previously calibrated on a Mettler-Toledo AX504 precision balance.

Figure 5 shows the output versus the corresponding input. The circles represent the experimental data acquired, which correspond to the five force steps exerted. The line represents the linear interpolation of those data. The balance shows high linearity (standard uncertainty of  $0.03 \mu\text{N}$ ) and a static sensitivity of  $0.123 \text{ V } \mu\text{N}^{-1}$  (the theoretical static sensitivity was  $0.1 \text{ V } \mu\text{N}^{-1}$ ).

#### 3.2. Noise floor test

The noise figure expressed by the balance was evaluated by noise floor tests. This kind of test is carried out in order to verify whether the balance is suitable for testing thrusters required to accurately control the spacecraft position. In fact, one of the strictest requirements on a thruster dedicated to precision missions is its noise figure. The intrinsic noise of the balance output sets a lower limit below which the thrust noise of the thruster cannot be measured.

During the noise floor tests, the output of the balance was recorded when no thrust force was exerted. The tests lasted up to 20 000 s with a sampling frequency of 50 Hz. Such a long time was required in order to detect the noise

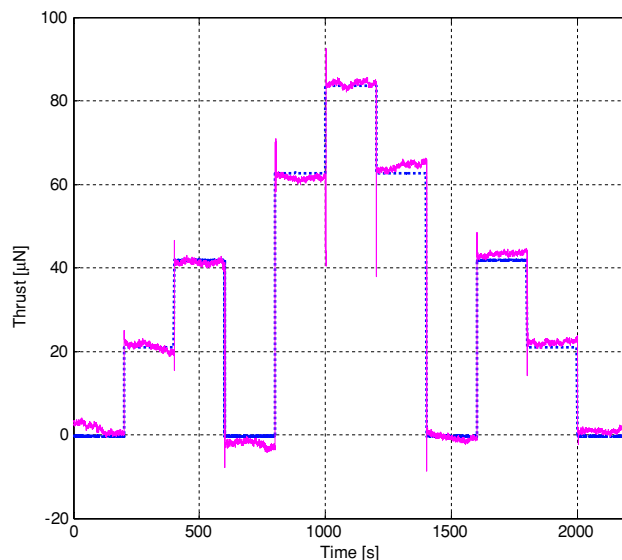


**Figure 6.** Noise spectral density of the balance output. Balance configuration with and without high-voltage cables.

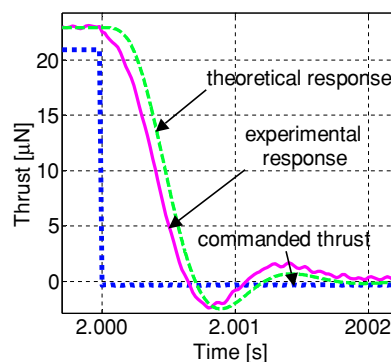
even at very low frequencies ( $10^{-4}$  Hz). In order to reduce the variance of the estimated periodogram, the noise spectral density was evaluated using the Welch averaged modified periodogram method of spectral estimation [13]. The input signal was divided into eight sections of equal length, each with 50% overlap. Any remaining entries that could not be included in the eight segments of equal length were discarded. Each segment was windowed with a Hamming window. A fast Fourier transform was applied to the windowed data. The modified periodogram of each windowed segment was computed. The set of modified periodograms was averaged to form the spectrum estimate. The resulting spectrum estimate was scaled to compute the power spectral density.

Figure 6 shows the noise spectral densities of the balance output in two different configurations. Both the tests were carried out in vacuum with the balance at a controlled temperature of 40 °C. This is the operative temperature of a FEEP thruster that uses caesium as propellant. The dark line represents the noise spectral density of the experimental configuration as shown in figure 2. The light line represents the noise spectral density of a configuration identical to the previous one, except that in this configuration the high-voltage cables were removed both from the thruster and from the dummy pendulum. The higher noise expressed by the configuration provided with high-voltage cables is caused by the asymmetric mechanical interference that those cables exerted on the pendula. In both cases, the noise spectral density increases at low frequencies. In order to be able to measure thrust satisfying LISA's requirements, balance developments seem necessary, including external noise reduction and the use of an active vibration damping system.

Noise floor tests were also carried out in different environments. The balance was positioned and tested directly on granite blocks, outside the vacuum chamber. Granite blocks are used in precision laboratories for vibration isolation. The balance was covered with a polystyrene box in order to prevent air convection disturbing the measurement. The noise generated in these conditions was comparable to that generated in the vacuum chamber. This fact suggests that vibrations transmitted from the ground are not a primary source of noise and that even acoustic vibrations play a role in generating noise. In this case, the isolation given by the vacuum chamber is better than that given by the polystyrene box.



**Figure 7.** Thrust test. Output signal: light line. Commanded thrust: dark dotted line.



**Figure 8.** Response to a step input. Experimental response, theoretical response and commanded thrust.

### 3.3. Thrust test

A known force history was exerted on the balance in order to verify its accuracy, resolution, range and dynamical response. The thrust range was limited to  $\pm 110 \mu\text{N}$  (or 0–220  $\mu\text{N}$ ) by the electronics of the balance (output range:  $\pm 14$  V). Figure 7 compares the commanded thrust with the balance output expressed in force units. The output was low-pass filtered at 1 Hz in order to exclude most of the noise. It was then detrended by removing offset and linear drift. Finally, it was converted from V into  $\mu\text{N}$  by dividing it by the static sensitivity determined during the calibration.

The balance output and the imposed force agree with a maximum difference of 4  $\mu\text{N}$ . The balance output shows a noise RMS of 1.1  $\mu\text{N}$ , which represents a limit for the resolution of the measurement.

### 3.4. Dynamic response

The dynamic response of the balance was tested and compared with the theoretical response given by the system described by the transfer function in (1). Figure 8 shows how the balance output follows a step input. The solid line represents the

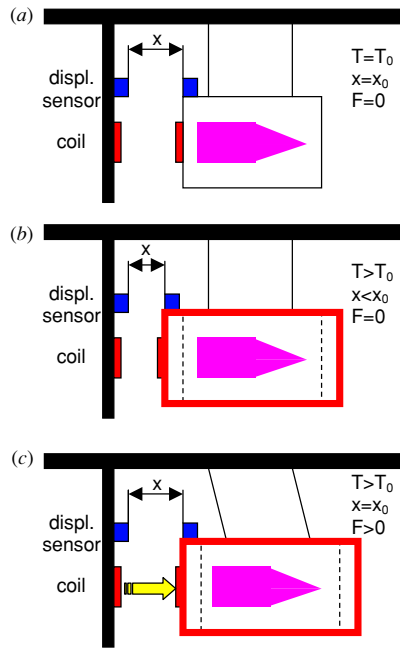


**Figure 9.** Thermal effect. (a) The pendulum is in its vertical position of equilibrium at  $T = T_0$  and  $x = x_0$ . (b) If the temperature increases ( $T > T_0$ ), the distance between the two parts of the displacement sensor decreases ( $x < x_0$ ). (c) The force feedback control restores the initial position ( $x = x_0$ ) exerting a force on the pendulum ( $F > 0$ ), which is read as thrust on the balance output.

output of the balance, the dashed line represents the theoretical response and the dotted line represents the estimated input. The balance responds with an underdamped oscillation with a settling time of about 2 s. The difference between the balance output and the theoretical response is less than  $1 \mu\text{N}$ , with a time shift of less than 0.1 s. This is an experimental confirmation of the dynamic model assumed and of the expected dynamic response of the balance (figure 4).

### 3.5. Temperature test

Temperature tests were required in order to predict possible disturbances caused by micro-thrusters in operational mode. In fact, local temperature gradients caused both by thruster heating and hot particle exhaust could produce unstable measurement of the thrust force. The balance proved to work efficiently at each constant temperature between  $20^\circ\text{C}$  and  $65^\circ\text{C}$ , which is the maximum temperature the balance is expected to reach.

However, tests showed that the balance was sensitive to temperature variation. Inducing thermal variations in the balance through halogen lamps causes thermal expansion of the Macor boxes that hold the thruster and the dummy. This causes a decrease of the distance ( $x$ ) detected by the displacement sensor (figures 9(a) and (b)). As a consequence, the force actuator exerts a force in order to restore the initial nulled position (figure 9(c)). The magnitude of the error generated is calculated by multiplying the coefficient of thermal expansion of Macor by half of the length of the box and then expressing the expansion in force units. The result shows an error of  $20 \mu\text{N } ^\circ\text{C}^{-1}$ . This figure has to be seen as the error in the output of the balance for each degree of

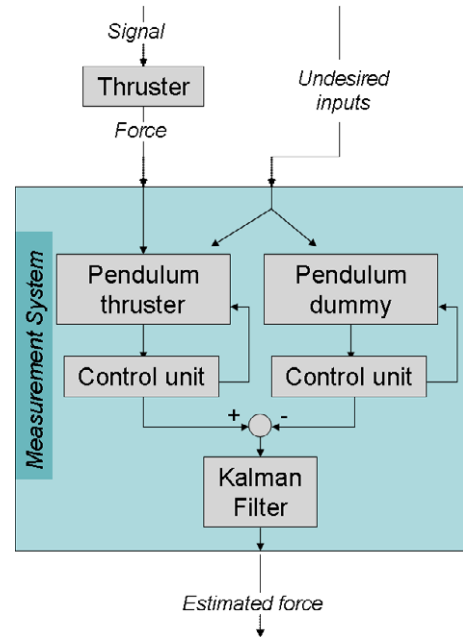


**Figure 10.** Block diagram of the measurement unit that includes the filtering process.

difference between the temperatures of the two boxes. In fact, if this process affected the thruster and the dummy sides of the balance in the same way, the output would not be affected.

The presence of the high-voltage power feeding cables contributes to worsening the temperature effect through three distinct mechanisms: (1) they are thought to be the highest source of asymmetry between the two sides of the balance. Therefore, even though the temperature changes in the same way on both sides, an error may appear because the same expansion on both sides will generate a different force. (2) They increase the stiffness of the pendulum, therefore the error of  $20 \mu\text{N } ^\circ\text{C}^{-1}$ , calculated neglecting the presence of the cables, is actually higher. (3) A variation of temperature on the cables may change their position and curvature, and thus the position of the pendula.

These considerations point to the choice of the box material and to the accommodation and choice of the high-voltage power feeding cables as sources of error in the measurement. If Macor were substituted by Zerodur, the measurement error would decrease from  $20 \mu\text{N } ^\circ\text{C}^{-1}$  to  $0.04 \mu\text{N } ^\circ\text{C}^{-1}$ . This is due to the very low coefficient of thermal expansion of Zerodur ( $0.05 \mu\text{m m}^{-1} ^\circ\text{C}^{-1}$ ).

## 4. Measurement estimate through Kalman filtering

The calibration phase showed that the compensation of the dummy pendulum was not sufficient to nullify all the effects of the undesired inputs and in particular those induced by environmental disturbances. Figure 6 shows, in fact, that the output of the balance is not null when the desired input (force from the thruster) is null. Filtering techniques were therefore considered in order to estimate the true input value of the balance. The noise process was represented in state space equations and an optimal estimate was performed through a linear minimum mean-square error (MMSE) filter [14].

Figure 10 shows the block diagram of the measurement system that includes the designed Kalman filter. The figure shows that the balance output was the input of the filter.

This study considered thrust forces changing slowly in time. The balance was thus analysed using a constant input of  $41.0 \pm 0.8 \mu\text{N}$  provided by an electric coil. The state space equations used to describe the constant input are [15]

$$\dot{x} = 0 \cdot x_1 + w_1 \quad y_1 = x_1 \quad (3)$$

where  $x_1$  is the state of the process and represents the true input provided to the balance,  $\dot{x}_1$  is the derivative of the state,  $y_1$  is the output of the process and  $w_1$  is the process model noise. The process noise was estimated to be  $2.5 \times 10^{-8} \mu\text{N}^2 \text{Hz}^{-1}$ , which is the noise associated with the solenoid/magnet force actuator used during experiments.

The dynamic response of the balance to noisy environmental disturbances was modelled using experimental data (figure 6) obtained for a null desired input (the solenoid/magnet actuator was switched off). The experimental balance output of figure 6 ( $S_{\text{out}}(i\omega)$ ) was low-pass filtered at 2 Hz as high-frequency responses were not of interest for micro-thrust measurements. The environmental disturbance was supposed to be a white noisy input and was thus modelled by a constant and unitary PSD ( $S_{\text{in}}(i\omega)$ ). Considering this hypothesis, the following general equation

$$S_{\text{out}}(i\omega) = G(i\omega) \cdot G(-i\omega) \cdot S_{\text{in}}(i\omega) \quad (4)$$

can be simplified as

$$S_{\text{out}}(i\omega) = G(i\omega) \cdot G(-i\omega). \quad (5)$$

If  $S_{\text{out}}(i\omega)$  is written as a partial-fraction expansion in the Laplace domain, equation (5) allows us to determine the shaping filter  $G(i\omega)$  [14] which represents the model of the balance to random environmental input. In order to compute  $G(i\omega)$ ,  $S_{\text{out}}(i\omega)$  (figure 6) was approximated using a class of partial-fraction expansions characterized by system variables with even exponents. Using a mean-square fitting procedure, the following function was obtained:

$$S_{\text{out}}(s) = \frac{0.0237}{-s^2 + 0.0028}. \quad (6)$$

Using (4) and (6), the transfer function of the balance to noisy environmental disturbances was computed:

$$G(s) = \frac{0.1539}{0.0529 + s}. \quad (7)$$

Equation (7) can be written in a canonical state space form [16]

$$\dot{x}_2 = 0.0529x_2 + w_2 \quad y_2 = -0.1539x_2 \quad (8)$$

where  $x_2$  is the state of the process,  $\dot{x}_2$  is the derivative of the state,  $w_2$  is the noisy input that was considered (environmental disturbance) and  $y_2$  is the value measured by the balance.

The complete model of the system considered both a constant input (true value) and a noise input (environmental disturbance). Thus, the output of the balance ( $y_b$ ) was computed by summing the two outputs of (3) and of (8) (as the linear range of the balance was considered, the superposition principle applied):

$$y_b = y_1 + y_2 + v \quad (9)$$

where  $v$  represents the measurement noise. The covariance associated with  $v$  was  $1 \text{ mV}^2$ .

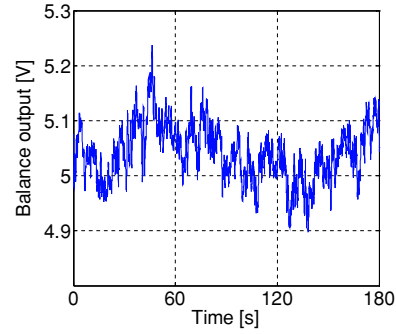


Figure 11. Data measured by the balance for a given constant input.

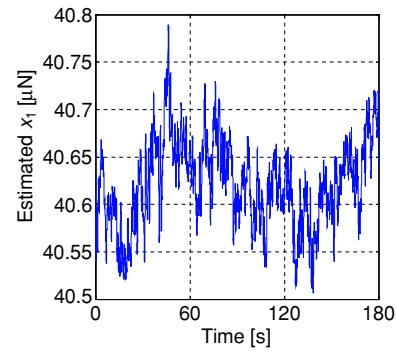


Figure 12. Estimated  $x_1$  (desired input).

To finalize the model of the system, the sensitivity value of the balance ( $cc = 0.123 \text{ V } \mu\text{N}^{-1}$ ) was introduced in (9):

$$y_b^* = cc \cdot (y_1 + y_2) + v^* \quad (10)$$

where  $v^*$  was expressed in volts. The final complete model obtained was thus

$$\begin{aligned} \dot{x}_1 &= 0x_1 + w_1 \\ \dot{x}_2 &= -0.0529x_2 + w_2 \\ y_b^* &= 0.123(x_1 + 0.1529x_2) + v^*. \end{aligned} \quad (11)$$

The model of the system was then discretized and used in the implementation of a Kalman filter [17].

The fundamental characteristic of the model, obtained by measurements of the balance (figure 6), is that the input of the system ( $x_1$ ) is one of the state variables of the model. Using the Kalman filter as an observer, all the state variables can be optimally estimated and thus the desired input too. The modelling described here made it possible to determine the input value of the balance from the noisy balance output and also to estimate both the disturbance ( $x_2$ ) and the measurement ( $y_b^*$ ).

The performance of the filter is shown in the test case presented in the following. A constant input equal to  $41.0 \pm 0.8 \mu\text{N}$  (95% level of confidence) was provided by the coil (desired input). The data measured by the balance ( $z$ ) are shown in figure 11 and vary between 4.89 V and 5.25 V. According to the block diagram of figure 10, these balance outputs entered in the filter which estimated the state variables of the system.

The first estimated state variable ( $x_1$ ) is presented in figure 12. The second state variable of the systems ( $x_2$ ) is presented in figure 13. Figure 12 shows the variable of main

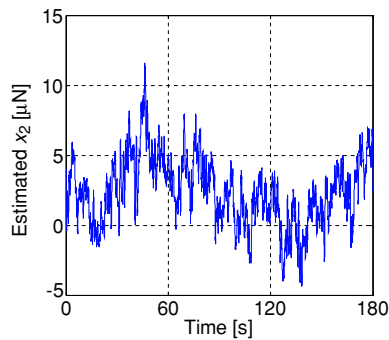


Figure 13. Estimated  $x_2$ .

interest: the estimated true value. As foreseen,  $x_1$  varies in the range of the predictable input. The implemented filter was able to reduce random disturbances and obtain measurements with a resolution of  $0.1 \mu\text{N}$ .

## 5. Uncertainty analysis

The output of the balance is affected by uncertainty, whose limits can be estimated by analysing the error sources. The main systematic error sources are related to the calibration chain. Ideally, the reference standard used for calibration should guarantee an uncertainty low enough that it is not necessary to consider it in the instrument uncertainty budget. This is not the case. The balance was calibrated using a solenoid/magnet force actuator, which was in turn calibrated using the Mettler-Toledo AX504 balance. The calibration of the micro-thrust balance gave a standard uncertainty of nonlinearity of  $0.3 \mu\text{N}$  (type A uncertainty evaluation). The calibration of the force actuator gave a standard uncertainty of 1% of the reading (type B). The calibration of the Mettler-Toledo balance gave a standard uncertainty of  $0.6 \mu\text{N}$  from the calibration sheet (type B). Other sources of systematic uncertainty were considered, namely thrust misalignment, data acquisition and force generated by currents (type B). They were evaluated, but their contributions were negligible.

Several error sources contribute to generating random uncertainty. These are: linear and rotational vibrations, tilt, temperature variations, data acquisition and signal processing. The last two are considered negligible. The others can be experimentally evaluated altogether considering the noise present in the balance output, which, as was seen previously, corresponds to a standard uncertainty of  $1.1 \mu\text{N}$  (type A).

The expanded uncertainty of the measurement can be calculated by root-sum-squaring the single components of standard uncertainty and then by multiplying the result by a coverage factor. For a level of confidence of 95%, the coverage factor is 2. The expanded uncertainty calculated in this way is a function of the value of the measurement. To be conservative, the higher limit is taken as the value of uncertainty over all the thrust range. Therefore, the expanded uncertainty with a level of confidence of 95% is  $3.3 \mu\text{N}$ .

## 6. Conclusions

The FEPP micro-thrust balance was calibrated and metrologically characterized in conditions close to the

operating conditions of a FEPP thruster. A mathematical dynamic model of the balance was also verified using test results. The balance showed a measurement range of  $0\text{--}220 \mu\text{N}$ , a sensitivity of  $0.123 \text{ V } \mu\text{N}^{-1}$ , a nonlinearity standard uncertainty of  $0.03 \mu\text{N}$ , a resolution of  $1.1 \mu\text{N}$  and an expanded measurement uncertainty of  $3.3 \mu\text{N}$ . A linear minimum mean-square error filter was implemented to reduce random disturbances and made it possible to perform measurements with a resolution of  $0.1 \mu\text{N}$ . Tests showed that a great part of the uncertainty could be improved by using a better calibration standard. An important noise source was related to the high-voltage cables necessary to feed the micro-thruster. A repositioning of the cables together with a reduction of their stiffness could significantly increase the accuracy of the balance. The balance also proved to be sensitive to temperature variation. A material with a low coefficient of thermal expansion (for example Zerodur) should replace Macor in the swinging boxes in order to improve the balance performance.

## Acknowledgments

The authors thank the ESA Propulsion Laboratory and the Ing. Aldo Gini Foundation for supporting the experiments.

## References

- [1] Toubol P and Rodrigues M 2001 The MICROSCOPE space mission *Class. Quantum Grav.* **18** 2487–98
- [2] LISA Study Team 2000 Laser Interferometer Space Antenna. A cornerstone mission for the observation of gravitational waves *ESA SCI* (11 July 2001)
- [3] Landgraf M, Hechler M and Kemble S 2005 Mission design for LISA Pathfinder *Class. Quantum Grav.* **22** 487–92
- [4] Fridlund C V M 2000 Darwin—the infrared space interferometry mission *ESA Bull.* **103** 20–5
- [5] Andrenucci M, Marcuccio S and Genovese A 1993 The use of FEPP systems for microNewton thrust level mission AIAA-93-2390
- [6] Mueller J 2000 Thruster options for microspacecraft: a review and evaluation of state-of-the-art and emerging technologies *Prog. Astro. Aero. AIAA* **187** 45–137
- [7] Ziemer J K 2001 Performance measurements using a sub-microNewton resolution thrust stand *Proc. 27th Int. Electric Prop. Conf. (Pasadena, CA)* IEPC-01-238
- [8] Merkwitz S M, Maghami P G, Sharma A, Willis W D and Zakrzewski C M 2002 A  $\mu\text{Newton}$  thrust stand for LISA *Class. Quantum Grav.* **19** 1745–50
- [9] Bonnet J, Marque J P and Ory M 2000 Development of a thrust balance in the microNewton range *Proc. 3rd Int. Conf. on Spacecraft Propulsion* ESA SP-465
- [10] Canuto E and Rolino A 2004 Nanobalance: an automated interferometric balance for micro-thrust measurement *ISA Trans.* **43** 169–87
- [11] Gamero-Castaño M 2003 A torsional balance for the characterization of microNewton thrusters *Rev. Sci. Instrum.* **74** 4509–15
- [12] Nicolini D, Chesta E, Gonzalez del Amo J, Saccoccia G, Hughes E B and Oldfield S 2001 FEPP-5 thrust validation in the  $10\text{--}100 \mu\text{N}$  range with a simple nulled-pendulum thrust stand: integration procedures *Proc. 27th Int. Electric Prop. Conf. (Pasadena, CA)* IEPC-01-288
- [13] Welch P D 1967 The use of fast Fourier transform for the estimation of power spectra: a method based on time averaging over short, modified periodograms *IEEE Trans. Audio Electroacoust.* **AU-15** 70–73

- [14] Brown R G and Hwang P Y C 1997 *Introduction to Random Signals and Applied Kalman Filtering* (New York: Wiley)
- [15] Welch G and Bishop G 1995 An introduction to the Kalman filter *Technical Report* TR95-041 (Chapel Hill, NC: University of North Carolina at Chapel Hill)
- [16] Nise N S 2003 *Control Systems Engineering* (New York: Wiley)
- [17] Ananthasayanam M 2004 A relook at the concepts and competence of the Kalman filter *Proc. 42nd AIAA Aerospace Sciences Meeting and Exhibit* (Reno, NV)